YALE
PEABODY
MUSEUM

JOURNAL OF MARINE RESEARCH

The *Journal of Marine Research,* one of the oldest journals in American marine science, published important peer-reviewed original research on a broad array of topics in physical, biological, and chemical oceanography vital to the academic oceanographic community in the long and rich tradition of the Sears Foundation for Marine Research at Yale University.

An archive of all issues from 1937 to 2021 (Volume 1–79) are available through EliScholar, a digital platform for scholarly publishing provided by Yale University Library at https://elischolar.library.yale.edu/.

Requests for permission to clear rights for use of this content should be directed to the authors, their estates, or other representatives. The *Journal of Marine Research* has no contact information beyond the affiliations listed in the published articles. We ask that you provide attribution to the *Journal of Marine Research.*

Yale University provides access to these materials for educational and research purposes only. Copyright or other proprietary rights to content contained in this document may be held by individuals or entities other than, or in addition to, Yale University. You are solely responsible for determining the ownership of the copyright, and for obtaining permission for your intended use. Yale University makes no warranty that your distribution, reproduction, or other use of these materials will not infringe the rights of third parties.

Long-period Waves over California's Continental Borderland[1]
Part I. Background Spectra

Frank E. Snodgrass, Walter H. Munk, and Gaylord R. Miller

Institute of Geophysics and Planetary Physics
University of California, San Diego

ABSTRACT

"Long" ocean waves, with frequencies between 0.2 and 10 cycles per hour (cph), have been recorded simultaneously at La Jolla on the California coast and at San Clemente Island, about 100 km seaward. The spectral power is greatest at the lowest frequencies but remains fairly uniform (about 5×10^{-2} cm²/cph) between 0.7 and 10 cph. Comparison of the Island and shore records shows that at the lowest frequencies (below 0.7 cph) the two records are consistently in phase and are highly coherent, as might be expected; above 0.7 cph they are out of phase, and the coherence is low. The phase reversal is fairly abrupt and suggests standing wave patterns, with the implication that the coast must be a good reflector. The failure of the coherence to recover after phase reversal suggests multiple modes, with an appreciable fraction of energy associated with in-phase modes even after most of the energy is out of phase. It is inferred that the observed waves are not only ones that cross the shelf from the deep sea but that comparable energy is present in "trapped" waves that have somehow been excited upon the shelf.

1. *Introduction.* For some time we have studied the low-frequency spectrum of ocean waves at coastal stations. These observations have focused our attention on the problem of whether the low-frequency wave energy is principally in the form of edge waves (or "trapped" modes or "discrete" modes) or whether the energy leaks in from the open sea and is part of the continuous spectrum. Wave observations at a single isolated station cannot provide a definite choice between these alternatives. One obvious experiment is comparison (in the frequency domain) of simultaneous recordings at two different stations. The present paper discusses such an experiment.

2. *The Experimental Site.* The continental borderland off southern California is shown in Fig. 1. Wave observations were made near the shore at La Jolla and at a point near San Clemente Island which is some 100 km from

3

the shore. Attention was paid to waves with frequencies in the range 0.2 to 10 cph.

An undulating shelf, occasionally a kilometer in depth, extends about 250 km seaward from La Jolla and then drops quickly away into deep water. Sections along the two lines marked A and B are shown in Fig. 5. The borderland is less wide toward the north. The Mexican territory to the south is not well surveyed.

3. *Instrumentation.* The wave pressures at each of the two stations were detected by a Vibrotron pressure gauge which has been described previously (Snodgrass, *et al.*, 1958); in outline, the water pressure changes the tension of a taut wire and so changes its natural frequency. The wire is maintained in oscillation by a constant voltage supplied from onshore, and the oscillation frequency is detected as a fluctuation in the electric current. In the present experiments it was necessary to attenuate the pressure changes due to the obvious short-period ocean waves, whose frequencies are typically 300 cph and upwards. Each Vibrotron was therefore enclosed in a hydraulic filter that attenuated such short-period fluctuations by a factor of 10^5 or more; this filter has been described by Snodgrass (1961).

Each instrument was laid in about 30 m of water and buried about one meter deep in the sea bottom to protect it from temperature fluctuations. The time occupied by 10^5 oscillations of the Vibrotron (about six seconds) was measured in microseconds and recorded digitally on punched paper tape. These measurements were made at intervals of 30 seconds, and the observations extended over about 90 hours. Thus the data consisted of about 11,000 pressure measurements at each station.

Two such experiments were made. Run A extended between 1200 on 13 October 1960 to 0230 on 17 October. Run B extended between 0745 on 17 October to 2400 on 24 October.

4. *Instrumental Noise.* The waves that are being studied are of such very small amplitude that it is necessary to make some comments on the observed "noise" level of the instruments. Thus, the spectral level in Fig. 2 averages only 0.05 cm²/cpks in the range from 0.2 to 8 cpks so that the total power in this band is only

$$(8 - 0.2)\ 0.5 \approx 0.4\ cm^2\ .$$

That is, the rms wave amplitude is only about 0.6 cm.

A Vibrotron instrument was capped to exclude all pressure variations, and a record from this capped instrument was made under conditions identical to those in the actual tests. The series consisted of 3000 numbers, and these diminished smoothly from 5,397,394 to 5,397,285, with only the last digit (the "least count") varying erratically by a unit value; for example, the last
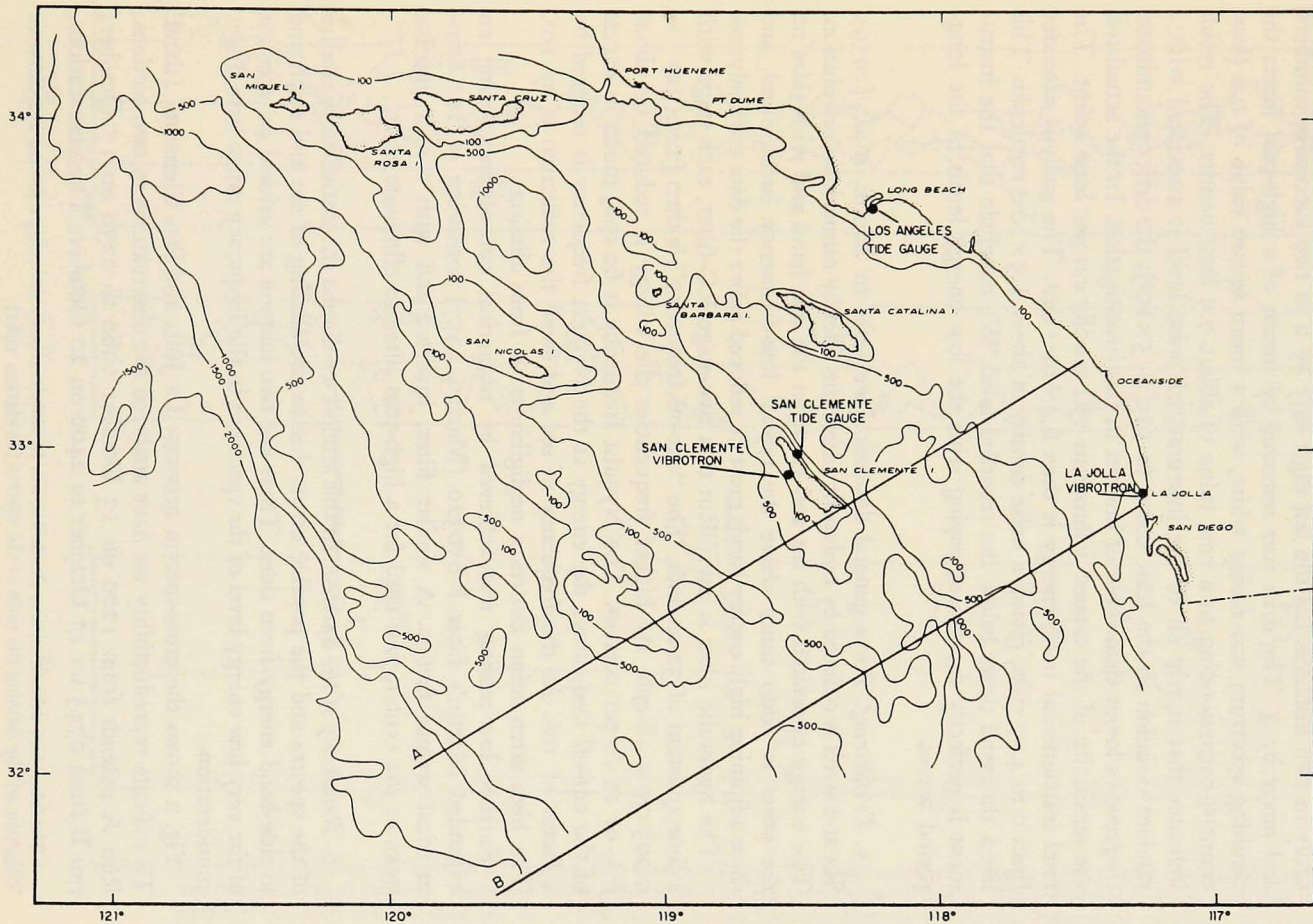
Figure 1. The continental borderland off southern California showing the location of the stations. The profiles along A and B are shown in Fig. 5.

two digits of the first ten numbers are 94, 93, 93, 94, 93, 94, 94, 94, 93, 94. Only in two instances did the last digit vary by 2 in two successive numbers, and never by 3. The drift was removed by means of a high-pass filter; the resulting spectrum was nearly white, with a mean square value of 0.2 (least count)^2, corresponding to a rms value of about 0.5 least counts. The result indicates that nearly all of the instrumental noise level is associated with a random variation in the least count (1 part in 5×10^6); the drift contaminates frequencies lower than those of interest in this investigation. In the actual test the sensitivity of the capped Vibrotrons was 0.0087 cm per least count. The total instrumental noise energy is then 6.4×10^{-5} cm^2. The analysis extended from 0 to 4.17 cpks, giving a noise density of about 1.5×10^{-5} cm^2/cpks. This lies a thousand times below the recorded level. We conclude that the instrument is perfectly capable of coping with the low energy levels of the long-period waves.

5. *Prefiltering.* For a general discussion we refer to Munk, *et al.*, (1959). Sea and swell is reduced by hydraulic filter, the tides by numerical convolution. The energy associated with sea and swell on the one hand and with tides on the other is 1000 times above the typical low-frequency background, and these adjoining high-energy bands must be reduced *before* the data are analyzed.

The hydraulic filter is equivalent to a two-stage RC-filter, each stage with a time constant of 32 seconds. The "cut-off frequency" is then $(2\pi \times 32)^{-1} =$ 0.005 cps = 18 cph. At higher frequencies the energy is reduced by about f^{-4}, or 12 db per octave[2]. The Nyquist frequency is 60 cph, much in excess of the cut-off frequency; the energy at the Nyquist frequency is reduced by a factor of 10^2. At the frequency of sea and swell the reduction is by 10^5. The high attenuation assures a negligible error from aliasing.

Further low-passing was achieved by numerical convolution, using an expanded Martin's filter P 050320 (Martin, 1957) consisting of 201 symmetrical weight factors. A similar filter, inverted and with a unit positive spike at the center, was used for a high-pass filter to eliminate tides.

6. *Reliability of the Spectra.* In this section we discuss the statistical reliability of the spectra and the possible errors due to the aliasing of sea and swell and to side-band energy from tides. These last two matters are critical on account of the very low energy level of the spectrum in the frequency range here under consideration.

Fig. 2 shows the cross-spectra between La Jolla and San Clemente Island. To indicate reproducibility we have analyzed the observations in two sections. Run A extends from 1200 on 13 October 1960 to 0230 on 17 October; run B from 0745 on 17 October to 2400 on 20 October. The observations,

---

[2] The laboratory calibration was checked *in situ* by simultaneously recording a filtered and unfiltered Vibrotron and by forming the ratio of the spectra (Snodgrass, 1961).
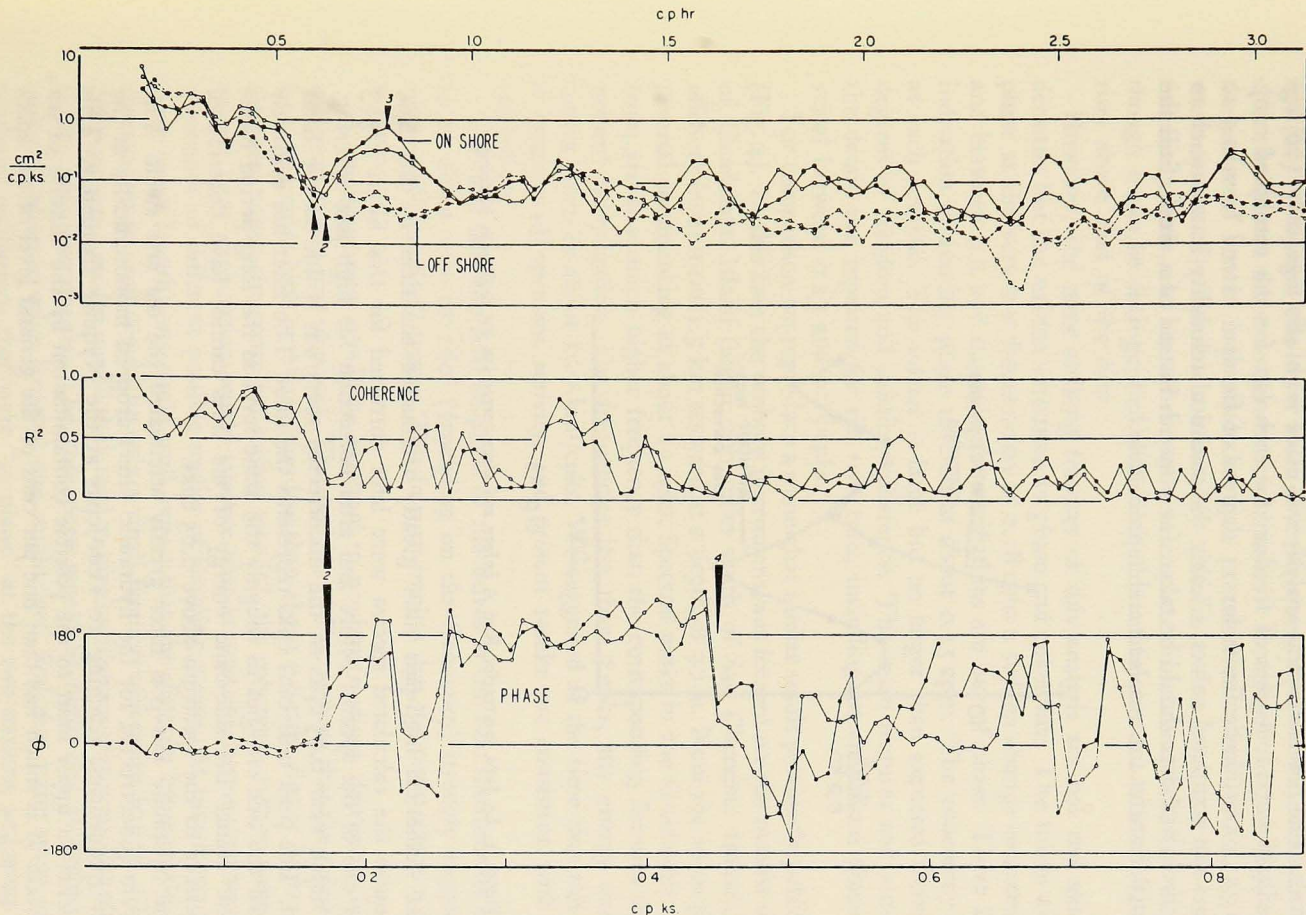
Figure 2. The observed cross-spectra between La Jolla and San Clemente Island. The upper curves show energy density for La Jolla (solid) and San Clemente Island (dashed). The closed circles refer to Run A, the open circles to Run B. The (coherence)² for the two runs is plotted in the center and the phase lead of La Jolla relative to San Clemente Island at the bottom. Frequencies are shown in cycles per hour (cph) and cycles per kilosecond (cpks). Spectra have been adjusted for hydraulic and numerical filtering. The features marked 1, 2, 3, 4 are marked for comparison with theoretical spectra, Figs. 10, 11, 12 (see text).

made at 30-second intervals, were low-passed, and decimated to 2-minute intervals. The power-spectral analysis was made with 480 lags (only 100 lags plotted), giving 11 degrees of freedom for each (22 for the combined run). The 95% confidence limits for 11 degrees of freedom extend from 0.5 to 3 times the computed values. Clearly the statistical reliability leaves much to be desired, and data should be taken for a month instead of a week. Still the essential features are resolved and reproducible.
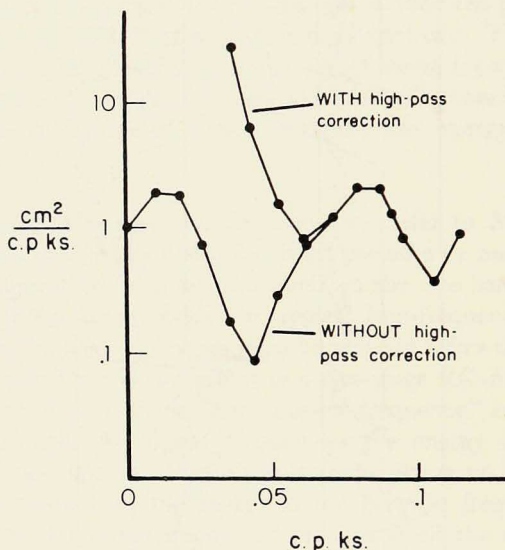

Figure 3. La Jolla spectra for Run A before and after correction for high-pass filtering.

The numerical high-pass filter greatly attenuated the tides in the data. Of course the calculated spectra were later corrected for this filter. Fig. 3 shows one of the spectra before and after correction for high-pass filtering. The notch near 0.05 cpks in the uncorrected spectrum is due to the filter action. The peak near 0.01 cpks represents the tides. The filter has evidently reduced the tide energies to roughly the same level as the long-period back-ground. Hence the side-band energy of the tides cannot have contributed appreciably to the spectrum above 0.05 cpks.

The hydraulic low-pass filter greatly attenuated the sea and swell. The spectrum (uncorrected for the hydraulic filter) dropped monotonically at the higher frequencies, reaching 10^{-4} cm²/cpks at the Nyquist frequency. This represents an upper limit to the possible contamination by the aliasing of sea and swell. It is much less than one per cent of the general level of the spectrum in Fig. 2.

7. *First Inferences from the Spectra.* All the spectra in Fig. 2 show a steep rise (as f-³) toward the lower limit of the frequency shown there. Above 0.17 cpks the spectra show no general trend in level though there are variations of the order of 10. It is possible that two processes contribute to the over-all wave system. One produces a sensibly uniform power level over the whole frequency scale, and the other produces a spectrum whose power falls as f-³, though it can be distinguished only at the lowest frequencies where its power rises above that of the first.

However, the most striking features of this analysis are not the spectral densities but the sudden variations in phase and coherence. The waves are in phase at the very low frequencies; at 0.18 cpks a sudden change commences; and between 0.2 and 0.4 cpks the oscillations are out of phase. There is an indication of another phase reversal at about 0.45 cpks. The coherency dips at each reversal. The scatter is large but no larger than expected from the degrees of freedom and existing coherence. The main features and some of the details are repeated for the two runs, including an anomalous phase reversal between 0.23 and 0.25 cpks.

For comparison we reproduce a somewhat similar result previously published (Fig. 4). In this case the onshore instrument was located on the eastern shore of Guadalupe Island (about 200 miles south of San Clemente Island), the offshore instrument 1.5 km seaward at a depth of 90 m. Note the sharp phase reversal commencing at about 12 cpks. Spectral peaks in the Guadalupe spectrum are at a much higher frequency than the corresponding features in the present investigation. For frequencies less than 5 cpks, the energy density settles down to about 10⁻² cm²/cpks. We suggested at the time that this was a measure of open-sea activity, and present results are consistent with this suggestion.

The fact that the relative phase of the waves at the two instruments tends to be either zero or 180° (depending on the frequency) strongly suggests a system of "standing" waves. This in turn implies that the coast acts as a good reflector.

A standing wave would be expected to produce motions that were highly coherent at any pair of places. The analyses in Fig. 2 show that the coherence is in fact quite high at frequencies less than about 0.6 cph. But at higher frequencies, when the phase has shifted to 180°, the coherence falls to quite low values. One explanation would suppose that at any one frequency there are a number of different possible modes of standing waves. At low frequencies (long wave length) one could well expect that the distance between the two observation stations would be only a small fraction of a wave length. All the different wave modes would then tend to give oscillations that were "in phase" at the two instruments. The coherence would be high. But at higher frequencies (shorter wave lengths) one might well find that some wave modes produced oscillations that were "in phase" at the two stations, and some pro-
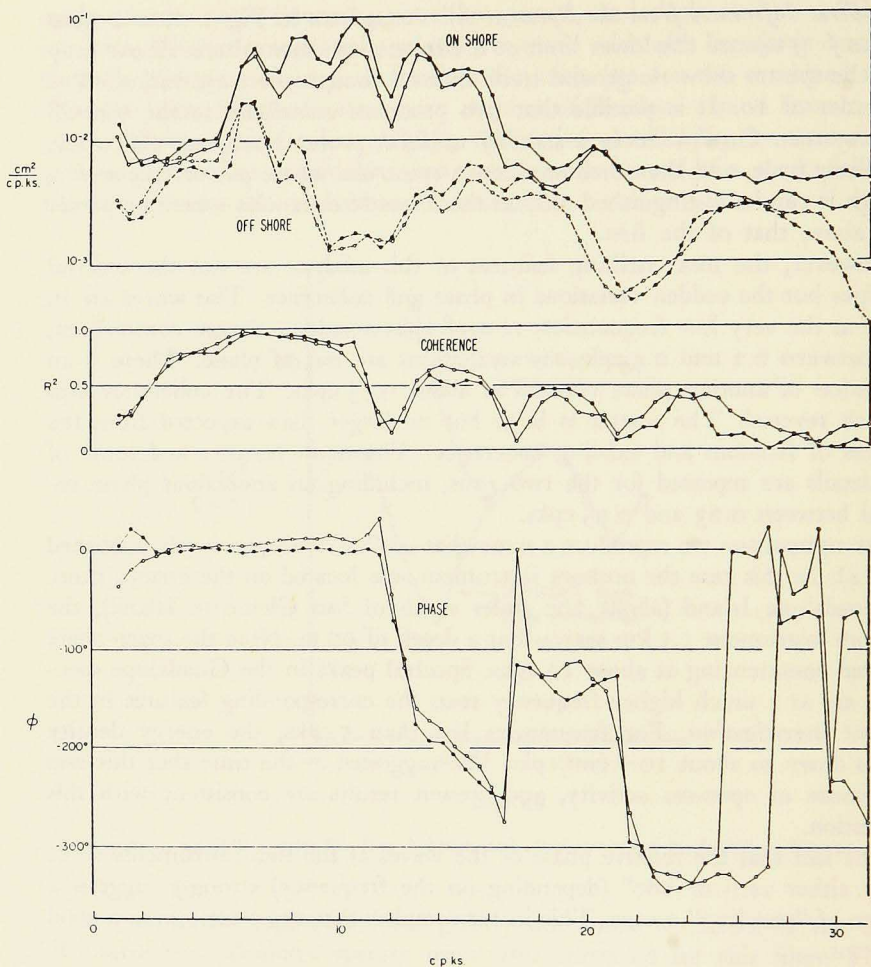
Figure 4. The cross-spectra between onshore and offshore recorders at the eastern side of Guadalupe Island (from Munk, *et al.*, 1959). The legend is analogous to that of Fig. 3. There are 126 degrees of freedom for each run (as compared to 11 in Fig. 3).

duced oscillations that were different in phase by $180°$. This would lead to a low coherence in the aggregate motions at the two stations.

The theoretical treatment that follows is a discussion of the various possible modes of standing waves. To explain the low coherence which is found experimentally, it is shown that one has to suppose that an appreciable fraction of the energy is contained in "trapped" modes that somehow develop on the continental shelf. That such "trapped" modes are a significant feature of the wave system is perhaps the most interesting outcome of the present experiments.
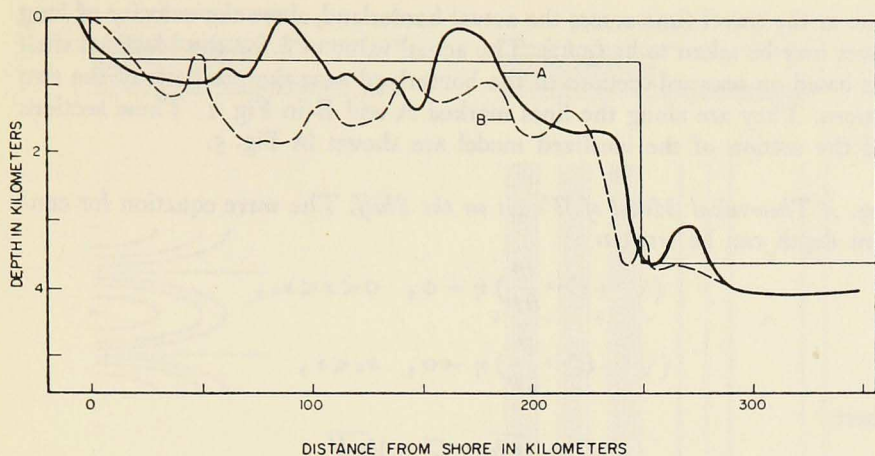
Figure 5. Depth profiles along the lines A and B indicated in Fig. 1. The theoretical estimates are based on the step-profile.

8. *An Idealized Topography.* To make a theoretical discussion, we have to idealize the actual situation. The form of the continental borderland has been shown in Fig. 1. We propose to idealize it into the form shown in Figs. 5 and 6. A straight steep coast (a perfect reflector) is bordered by a shelf of uniform depth and width, and this in turn flanks a deeper sea. This model is unrealistic in the sense that it supposes that the shelf has a uniform width, but a more complicated model would scarcely be tractable. The undulations in the bottom of the actual borderland are not perhaps very important when one is considering very long waves. The idealized shelf has been given a depth h found by making $h^{-\frac{1}{2}}$ equal to the mean value of (true depth)$^{-\frac{1}{2}}$. By this means we insure that the travel time of waves across the idealized shelf is the
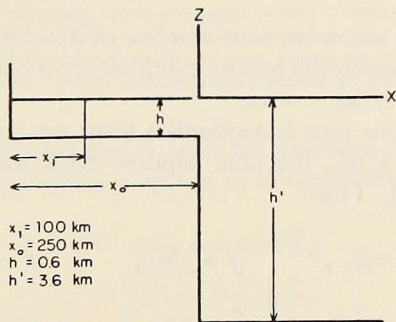

Figure 6. The coordinate system is centered at the sea surface along the coastline, with x pointing seaward, z upward. The coordinate y (not shown) is parallel to shore into the paper. The San Clemente recorder is at x_I, the offshore "cliff" at x_0.

same as the travel time across the actual borderland, since the velocity of long waves may be taken to be $(g\,h)^{\frac{1}{2}}$. The actual value of h for the idealized shelf was based on seaward sections of the borderland near the positions of the two stations. They are along the lines marked A and B in Fig. 1. These sections and the section of the idealized model are shown in Fig. 5.

9. *A Theoretical Model of Waves on the Shelf.* The wave equation for constant depth can be written

$$\left(\nabla^2 + C^{-2}\frac{\partial^2}{\partial t^2}\right)\eta = 0, \quad 0 \leqslant x \leqslant x_0,$$

$$\left(\nabla^2 + C'^{-2}\frac{\partial^2}{\partial t^2}\right)\eta = 0, \quad x_0 \leqslant x,$$

where

$$C = \sqrt{g\,h}, \quad C' = \sqrt{g\,h'}$$

designate the velocities on and off the shelf, respectively; and where η is the surface elevation as a function of time, t. We seek solutions of the form

$$\eta = a\cos mx \cos(ny - \omega t + \varphi), \quad 0 < x \leqslant x_0,$$

and these represent waves traveling in the y-direction (along shore) with crests and troughs *normal* to shore (Fig. 7). We may consider these standing waves as a superposition of an incident and reflected wave,

$$\eta = \tfrac{1}{2}a\cos(mx + ny - \omega t) + \tfrac{1}{2}a\cos(-mx + ny - \omega t),$$

where $m = k\cos\theta$ and $n = k\sin\theta$ are the components of the wave number, $k = \omega/C$, and θ is the incident direction on the shelf.

At the coastline the velocity component u normal to shore vanishes so that $\partial\eta/\partial x = 0$ at $x = 0$.

At the cliff, conservation of mass implies continuity in hu or $(h \cdot \partial\eta/\partial x)$, and conservation of momentum implies continuity in $\partial\eta/\partial z$. Thus $h\,(\partial\eta/\partial x) = h'\,(\partial\eta'/\partial x)$, and $\eta = \eta'$ at $x = x_0$.

To put the equations into dimensionless form we refer all distances to x_0 and all times to $t_0 = x_0/C$, the time required for a wave to travel over the shelf $(t_0 = 0.9$ hours). Thus

$$\widehat{x} = x/x_0, \qquad \widehat{y} = y/x_0, \qquad \widehat{t} = t/t_0,$$

$$\widehat{m} = mx_0, \qquad \widehat{n} = nx_0, \qquad \widehat{\omega} = \omega t_0,$$

and

$$\eta = a\cos\widehat{m}\,\widehat{x}\cos(\widehat{n}\,\widehat{y} - \widehat{\omega}\,\widehat{t} + \varphi). \tag{1}$$
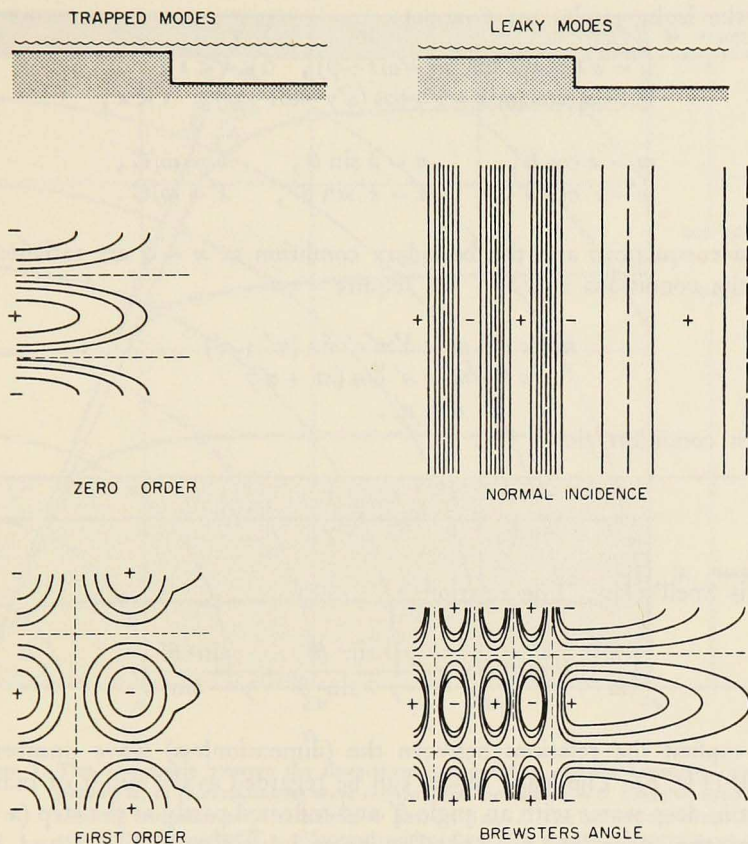
Figure 7. Schematic presentation of leaky (right) and trapped (left) shelf waves. The lines are con-
tours of equal elevation (or depression) of water level relative to the undisturbed level.
Only one complete wave length in the direction parallel to shore is shown. The pattern
repeats itself indefinitely and is propagated parallel to shore (up or down on the paper).
For the case of leaky modes the two cases correspond to normal incidence and "Brewster
incidence." For the trapped modes we have plotted the fundamental ($j = 0$) and first
harmonic ($j = 1$). Various normal-to-shore profiles are plotted in Fig. 11.

From now on we shall drop the $\wedge$ with the understanding that unless other-
wise stated all quantities (except η) are in dimensionless form.

Note that

$$f \text{ in cpks} = 0.049 \, \widehat{\omega},$$

$$f \text{ in cph} = 0.175 \, \widehat{\omega}.$$

There are two classes of solutions (Fig. 7): the leaky modes and the trapped
modes. The former are trigonometric offshore, the latter decay exponentially
offshore (hence the name "edge waves").

For the leaky modes we now set

$$\eta = a \cos mx \cos (ny - \omega t + \varphi), \quad 0 \leqslant x \leqslant 1,$$
$$\eta' = a' \cos (m'x + \alpha') \cos (n'y - \omega t + \varphi), \quad 1 \leqslant x,$$

(2)

with

$$m = k \cos \theta, \qquad n = k \sin \theta, \qquad k = \omega/C,$$
$$m' = k' \cos \theta', \qquad n' = k' \sin \theta', \qquad k' = \omega/C.$$

The wave equations and the boundary condition at $x = 0$ are satisfied. To satisfy the conditions at $x = 1$ we require

$$h\,m\,a \sin m = h'm'a' \sin (m' + \alpha')$$
$$a \cos m = a' \cos (m' + \alpha')$$
$$n = n'.$$

(3)

The last condition yields

$$\frac{\sin \theta}{\sin \theta'} = \frac{k'}{k} = \frac{C}{C'} = \frac{1}{\gamma} \quad \text{(say)},$$

which is Snell's law. The relation

$$\left(\frac{n}{m}\right)^2 = \tan^2 \theta = \frac{\gamma^{-2} \sin^2 \theta}{1 - \gamma^{-2} \sin^2 \theta'} = \frac{\sin^2 \theta'}{\gamma^2 - \sin^2 \theta'}$$

(4)

makes explicit the relations between the (dimensionless) wave numbers on the shelf (Fig. 8). The leaky modes can be regarded as the result of radiation incident in deep water with an angle θ' and reflected partly at the step $(x = 1)$, partly at the shore line $(x = 0)$. For normal incidence, $\theta' = 0$ and hence $n = 0$: the wave length along shore is infinite. For glancing incidence, $\theta' = 90°$ and hence $n^2 = m^2/(\gamma^2 - 1)$. On Fig. 8, any point contained between the radial lines corresponding to normal and glancing incidence is a legitimate solution: the spectrum is *continuous* for the leaky modes. Incidence at Brewster's angle, $\tan \theta' = \gamma$, leads to $n = m \cot \theta' = m/\gamma$ and is of special interest.

For the trapped waves we set

$$\eta = a \cos mx \cos (ny - \omega t + \varphi), \quad 0 \leqslant x \leqslant 1,$$
$$\eta' = a' \exp (-m'x) \cos (ny - \omega t + \varphi), \quad 1 \leqslant x.$$

The wave equations then yield

$$m^2 + n^2 = k^2, \quad -m'^2 + n^2 = k'^2$$

and the boundary condition at $x = 1$ yields

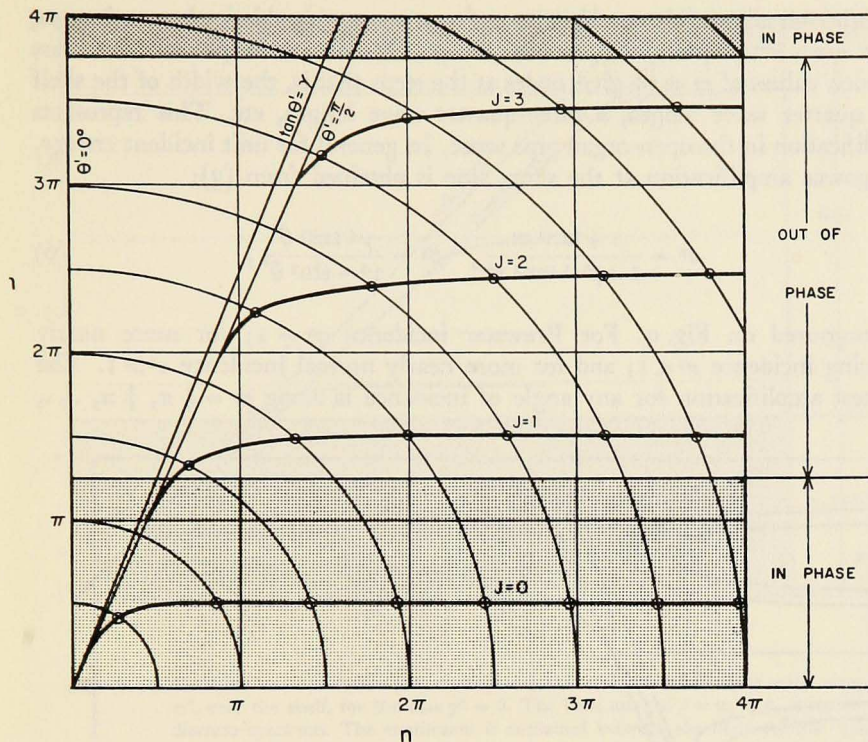$$a \cos m = a'e^{-m'}, \quad h\,m\,a \sin m = h'm'a'e^{-m'}.$$

Figure 8. The relationship between the along-shore component, n, and the normal-to-shore component, m, of (dimensionless) wave numbers for the case $\gamma^2 = 6$. Lines of equal (dimensionless) frequency are drawn for $\omega = \frac{1}{2}\pi$, π, $\frac{3}{2}\pi$, ... The continuum is contained between the rays marked $\theta' = 0°$ (normal incidence) and $\theta' = \frac{1}{2}\pi$ (glancing incidence). Discrete modes are drawn for modal numbers $j = 0$, 1, 2, 3. The shaded portions refer to such values of m for which a coastal instrument and a recorder at $x = 0.4$ are in phase.

The three equations can be combined to

$$m^2 \left(\tan^2 m + \gamma^2\right) = n^2 \gamma^2 \left(\gamma^2 - 1\right), \tag{5}$$

and the spectrum is accordingly *discrete*. The first four modes are shown. For all but the fundamental mode there is a lower limit to the permissible frequencies and wave numbers. For the j'th mode, the cut-off wave number is derived by substituting $n^2 = m^2/(\gamma^2 - 1)$ for glancing incidence into (5). The result is

$$\tan m = 0, \quad m_j = j\pi, \quad j = 0, 1, 2, \ldots.$$

Lines of equal frequency lie on the circles $m^2 + n^2 = \omega^2$, and accordingly the cut-off frequencies are given by

$$\omega_j = \left(1 - \gamma^{-2}\right)^{-\frac{1}{2}} m_j.$$

Although all possible combinations of m, n are permissable in the continuum, there are certain parts favored over others. Maximum amplification occurs for such values of m as to give nodes at the step; that is, the width of the shelf is a quarter wave length, a three-quarter wave length, etc. This represents amplification in the open-organ pipe sense. In general for unit incident energy, the power amplification at the shore line is obtained from (3):

$$a^2 = \frac{1 + \tan^2 m}{1 + \beta^{-2} \tan^2 m}, \quad \beta^2 = \frac{\gamma^4 \cos^2 \theta'}{\gamma^2 - \sin^2 \theta'}, \tag{6}$$

as contoured on Fig. 9. For Brewster incidence $a^2 = 1$; for more nearly glancing incidence $a^2 \leqslant 1$; and for more nearly normal incidence $a^2 \geqslant 1$. The greatest amplification for any angle of incidence is along $m = \frac{1}{2} \pi, \frac{3}{2} \pi, \ldots,$
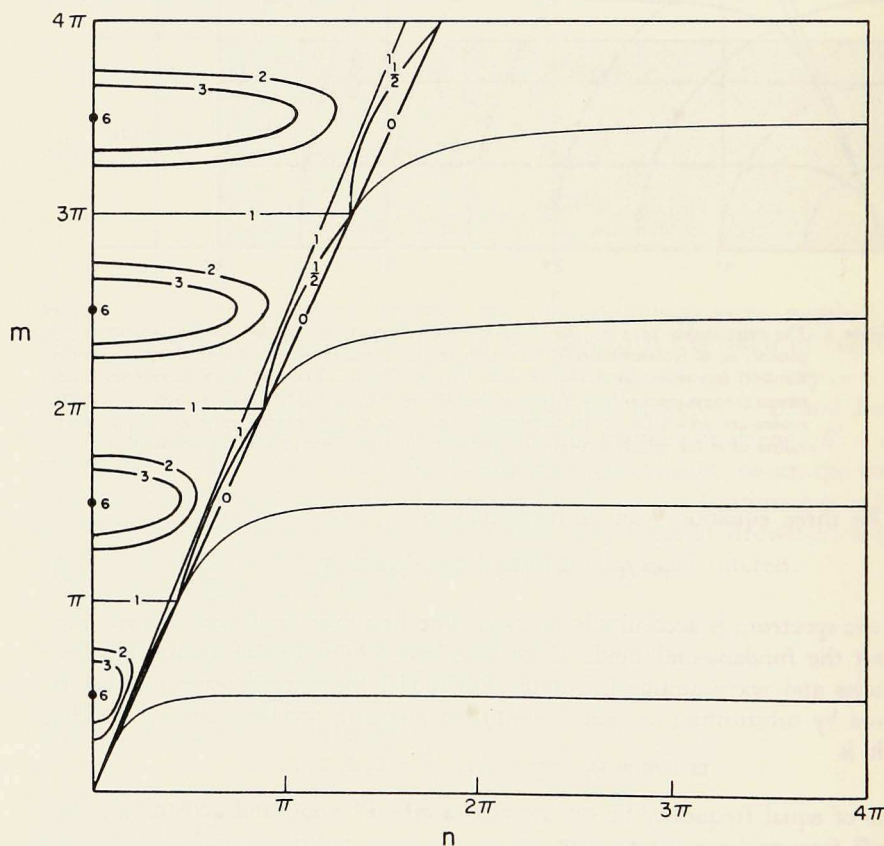

Figure 9. Contours of equal energy, a^2, at $x = 0$ unit incident energy, superimposed on the wave-number diagram (Fig. 8). Contours are shown for $a^2 = 0, \frac{1}{2}, 1, 2, 3,$ and $6 (= \gamma^2)$.
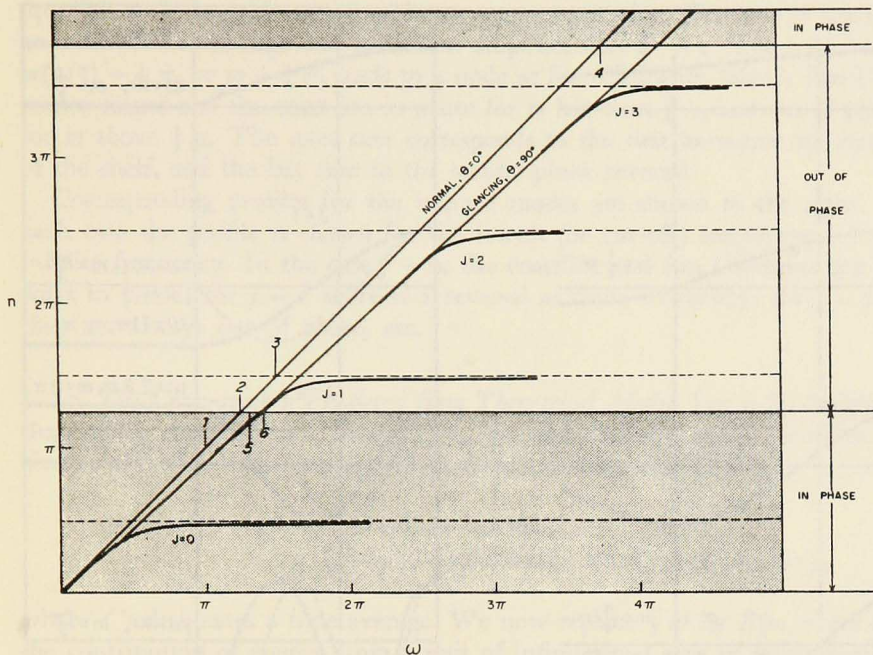
Figure 10. Relation between dimensionless frequency, ω, and normal-to-shore wave component, m', over the shelf, for the case $\gamma^2 = 6$. The lines marked $j = 0$, 1, 2, 3 represent the discrete spectrum. The continuum is contained between the lines marked "glancing" and "normal" incidence. Resonance occurs at $m = \frac{1}{2}\pi$, $\frac{3}{2}\pi$, $\frac{5}{2}\pi$, ... and antiresonance at $m = \pi$, 2π, 3π. For the case $x = 0.4$ phase reversals occur at $m = \frac{5}{4}\pi$, $\frac{15}{4}\pi$, ... as indicated. The points marked 1, 2, ... refer to similar markings in Figs. 2, 11 and 12.

and equals $a^2 = \beta^2$. The amplification is a maximum for normal incidences, $a^2 = \beta^2 = \gamma^2$.

It is not possible to draw an equivalent amplification diagram for the discrete spectrum, for here the amplitude offshore approaches zero. But we may interpret the lines as knife edges, infinitely narrow and infinitely high.

For some purposes it is more convenient to plot these relations in ω, m-space (Fig. 10). Lines of equal n are along the equilateral hyperbola

$$\omega^2 - m^2 = n^2 . \tag{7}$$

Fig. 11 shows profiles of the water surface normal to shore for certain selected situations. On the left are plotted the profiles of the leaky modes. The upper figure corresponds to a frequency so low (and a length so long) that the wave is hardly affected by the existence of the shelf. The next case, $m = \frac{1}{2}\pi$, corresponds to a node at the outer edge of the shelf, leading to maximum amplification at the shore line. This is analogous to the fundamental
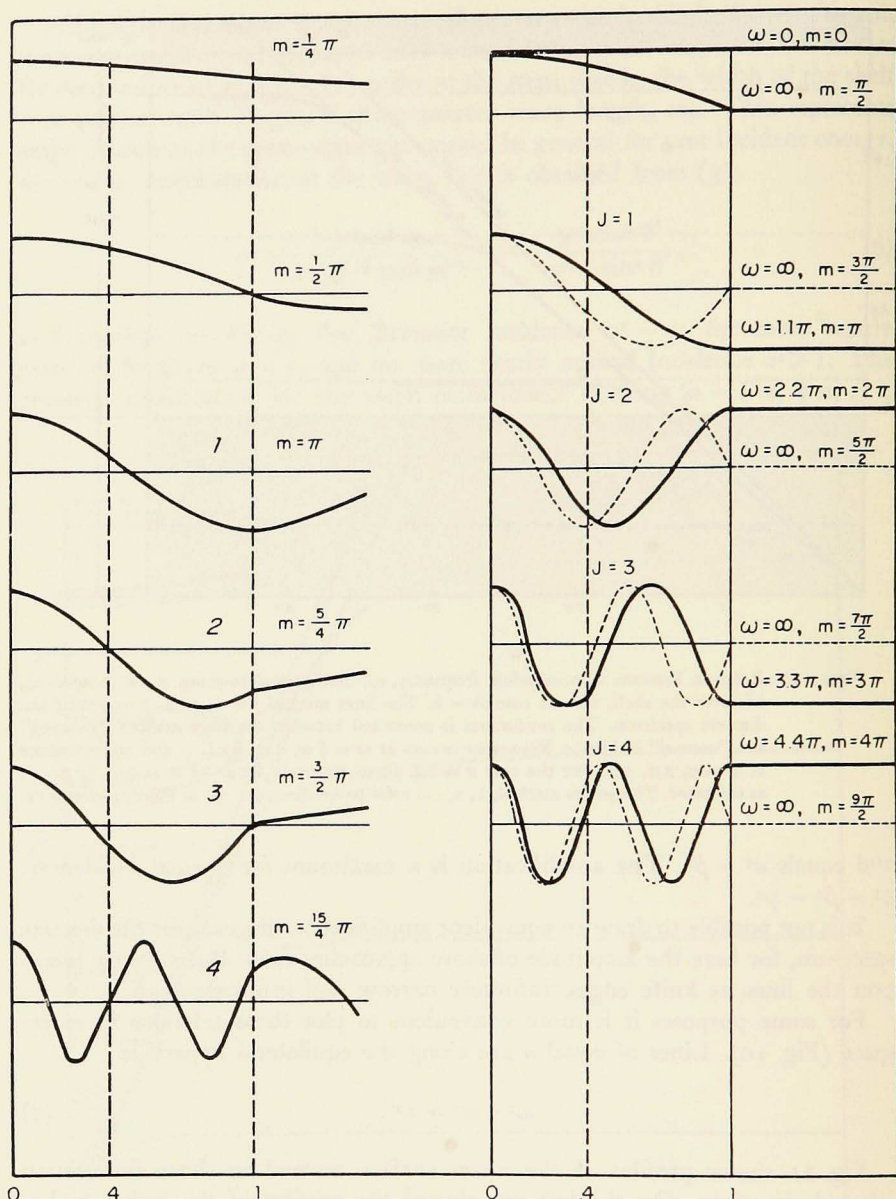
Figure 11. Theoretical profiles of the sea surface normal to shore. The shore line is at $x = 0$, San Clemente at $x = 0.4$, and the outer edge of the shelf at $x = 1$ (see Fig. 6). All profiles are normalized to unit amplitude at the coast line, hence to amplitude a^{-1} at antinodes off the shelf. The left figures give the leaky modes. The right figures correspond to the trapped modes of the lowest three orders; in each case the profile is plotted for the lowest and highest frequencies at which these modes can exist. The numbers 1, 2, 3, 4 refer to similar markings on Figs. 2, 10, and 12.

(quarter wave length) resonance in an open organ pipe. For $m = \pi$ there is an antinode at the edge and minimum amplification: $a^2 = 1$. The case $mx = m(2/5) = \frac{1}{2}\pi$, or $m = \frac{5}{4}\pi$, leads to a node at San Clemente Island: San Clemente Island and the coast are in phase for m less than $\frac{5}{4}\pi$, and out of phase for m above $\frac{5}{4}\pi$. The next case corresponds to the first harmonic resonance of the shelf, and the last case to the second phase reversal.

Corresponding profiles for the trapped modes are shown to the right. In each case the profile is shown for the lowest (or cut-off) frequency and for infinite frequency. In the case $j = 0$, the coastline and San Clemente are always in phase; for $j = 1$ there is a reversal at some frequency; for $j = 2, 3$ they are always out of phase, etc.

10. *The Cross-spectra Predicted from Theoretical Model.* Let $\eta_1(t)$ designate the surface elevation at a location, x_1, y_1; and similarly $\eta_2(t)$. Consider an elementary wave train (eq. 1) and perform the cross-correlation

$$\langle \eta_1(t)\, \eta_2(t-\tau) \rangle = \tfrac{1}{2}\, a^2 \cos mx_1 \cos mx_2$$
$$[\cos n(y_2-y_1) \cos \omega\tau + \sin n(y_2-y_1) \sin \omega\tau]\,,$$

where $\langle \rangle$ designates a time average. We now replace $\frac{1}{2} a^2$ by $E(m, n)\delta m\, \delta n$, the contribution of energy from a unit of infinitesimal area in wave-number space. Inasmuch as we have assumed random and uncorrelated phases, φ, between elementary wave trains, we can write for the correlation from all possible waves

$$R_{12}(\tau) = \int_{-\infty}^{\infty}\int_{-\infty}^{\infty} E(m, n) \cos mx_1 \cos mx_2$$
$$[\cos n(y_2-y_1) \cos \omega\tau + \sin n(y_2-y_1) \sin \omega\tau]\, dm\, dn\,.$$

In a similar manner we can express $R_{12}(\tau)$ in terms of contribution $E'(\omega, m)\, \delta\omega\, \delta m$ from elementary areas in an ω, m-diagram (Fig. 9):

$$R_{12}(\tau) = \int_{-\infty}^{\infty}\int_{-\infty}^{\infty} E'(\omega, m) \cos mx_1 \cos mx_2$$
$$[\cos n(y_2-y_1) \cos \omega\tau + \sin n(y_2-y_1) \sin \omega\tau]\, dm\, d\omega\,,$$

with $n = n(\omega, m)$ in accordance with (7). E and E' are not the same. The relation is given by $E\, dm\, dn = E'\, d\omega\, dm$, and hence

$$E' = E\, \mathcal{J}\left(\frac{m, n}{m, \omega}\right) = E\frac{\omega}{n}\,. \tag{8}$$

The measured quantities are the corresponding Fourier transforms:

$$S_{11}(\omega) = R_{11}(\tau) \cos \omega\tau \, d\tau = \int E'(\omega, m) \cos^2 mx_1 \, dm \, ,$$

$$S_{22}(\omega) = R_{22}(\tau) \cos \omega\tau \, d\tau = \int E'(\omega, m) \cos^2 mx_2 \, dm \, ,$$

$$C_{12}(\omega) = R_{12}(\tau) \cos \omega\tau \, d\tau = \int E'(\omega, m) \cos mx_1 \cos mx_2 \cos n(y_2 - y_1) \, dm \, ,$$

$$Q_{12}(\omega) = R_{12}(\tau) \sin \omega\tau \, d\tau = \int E'(\omega, m) \cos mx_1 \cos mx_2 \sin n(y_2 - y_1) \, dm \, .$$

Again $n = n(m, \omega)$ in accordance with (7). If we wish to interpret the computed quantities in terms of energy density in wave-number space, then we make use of (8) to write

$$S_{11}(\omega) = E(m, n) \frac{\omega}{n} \cos^2 mx_1 \, dm \, ;$$

and similarly for S_{22}, C_{12}, and Q_{12}. The integration is along the circles $\omega =$ constant (Fig. 8).

Phase and coherence are defined by the relations

$$\tan \varphi = \frac{Q_{12}}{C_{12}}, \quad R^2 = \frac{C^2_{12} + Q^2_{12}}{S_{11} S_{22}} \, .$$

For the case $y_1 = y_2$, we have $Q_{12} = 0$ and $\varphi = 0°$ or $180°$ according to whether

$$C_{12} = \int E'(\omega, m) \cos mx_1 \cos mx_2 \, dm$$

is positive or negative.

The foregoing discussion follows the usual lines for determining two-dimensional wave spectra with the following important difference: in the usual formulation the cross-spectra depend only on the separations, $x_2 - x_1$ and $y_2 - y_1$. This is still assumed to hold along the y-axis, but not along the x-axis. The reason is that the coast acts as a coherent reflector, producing non-random phase relations.

11. *Comparison of Theory and Experiment.* Let $\frac{1}{2} S(f)$ designate the frequency spectrum of waves normally incident from deep water. Then $S(f)$ is the deep-water spectrum at the antinodes, and

$$a^2(f) S(f), \quad a^2 \cos^2(mx_1) S(f) \, ,$$

are the associated spectra at the shore line ($x = 0$) and at San Clemente Island ($x = x_1$), respectively. For this case of normal incidence, $m = \omega = 2\pi f$ and $a^2 = [1 + \tan^2 m][1 + \gamma^{-2} \tan^2 m]^{-1}$. In Fig. 12 we have drawn the theoretical spectra normalized to $S(f) = 1$. For the present model of normal incidence, the phase reverses abruptly, and the coherence drops to zero and then immediately recovers. Successive resonance peaks are all of equal amplitude. In
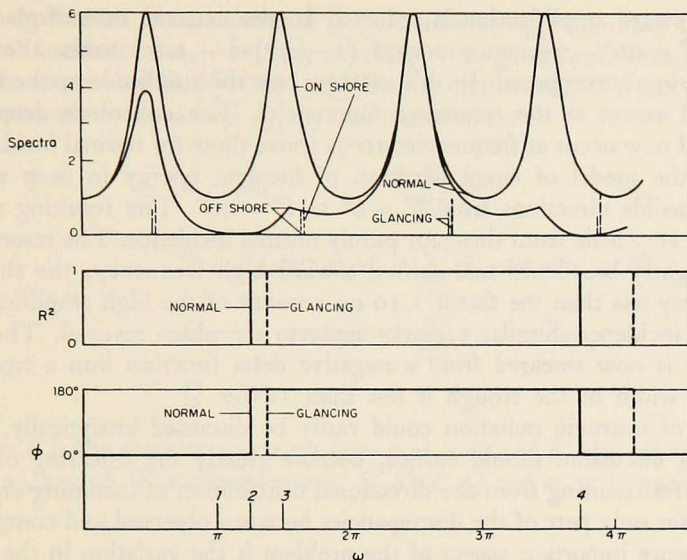
Figure 12. Theoretical spectra for the geometry of Fig. 6, for normal incidence (solid) and glancing incidence (dashed). The numbers 1, 2, 3, 4 refer to similar markings on Figs. 2, 10, and 11.

these respects, and in others, the theoretical spectra differ very considerably from the observed spectra (Fig. 2). The features that can perhaps be compared are the following:

Numbered features on Figs. 2, 9, 10, 11	Feature	Frequency ω Observed	Computed
(1)	Spectral minimum	3.4	3.14
(2)	Minimum in San Clemente spectrum, drop of coherence and phase reversal	3.7	3.93
(3)	La Jolla spectra peak	4.5	4.72
(4)	Second phase reversal	9.2	11.7

Computed and observed frequencies are in fair agreement except for the second phase reversal. It is disturbing that there is no clear indication of the fundamental resonance peak in the observed spectra and that the coherence recovers so little after the first phase reversal. The separation between the La Jolla and San Clemente spectra occur roughly as predicted (note that the energy scale is logarithmic in Fig. 2 and linear in Fig. 12). The width of the resonance peak is about right: according to theory $Q = \gamma^2 = 6$; the observed Q lies between 4 and 7.

For incidence other than normal ($\theta' = 0°$), the resonance peaks (and anti resonances) shift toward higher frequencies by a factor $(1 - \gamma^{-2} \sin^2 \theta')^{\frac{1}{2}}$,

and the shoreward amplification is reduced. In the extreme case of glancing incidence ($\theta' = 90°$), resonance occurs $(1 - \gamma^{-2})^{-\frac{1}{2}} = 1.10$ times the frequencies previously computed. In this extreme case the amplitude at the shore line vanished except at the resonance frequencies. The coherence drop and phase reversal now occur at frequencies 10% above those for normal incidence.

Consider the model of equal partition of incident energy in deep water among all possible directions from $\theta' = 0°$ to $\theta' = 90°$. The resulting shore spectra differ very little from those for purely normal incidence. The resonance peaks are slightly broadened and shifted toward high frequency; the shift is by considerably less than the factor 1.10 on account of the high amplification near normal incidence. Similar remarks apply to the phase reversal. The dip in coherence is now smeared from a negative delta function into a trough; the effective width of the trough is less than 10%.

The case of isotropic radiation could easily be discussed analytically. But the foregoing discussion should suffice, because clearly the smearing of the spectral features resulting from the directional distribution of incoming energy can account for only part of the discrepancies between observed and computed features. A more important aspect of the problem is the variation in the bottom topography in a direction parallel to the coastline. Here we are not emphasizing the Island and other relatively small-scale features; these are short as compared to the wave length of the gravest modes, and their principal effect is in scattering wave energy. The important aspect is the variation in the over-all dimension of the borderland as we move up or down the coast by a distance of wave length. Perhaps the absence of a pronounced peak corresponding to the gravest mode (wave length $4x_0 = 1000$ km) as compared to the first harmonic (wave length $\frac{1}{3} \times 1000$ km) is related to the very considerable variation in the borderland over the distance of 1000 km. In all events this variation along the coast must be an important factor in smearing the theoretical features and reducing coherence. The associated three-dimensional analysis has not been attempted.

MULTIPLE MODES. The discussion so far indicates that some of the gross features can be interpreted in terms of radiation incident from the open sea. But some of the observed features are definitely beyond the scope of this abbreviated treatment, and we need to develop some insight into the effect of multiple modes on coherence and phase.

In ω, m-space (Fig. 10) the discrete spectrum is concentrated along the modal lines

$$m = m_j(\omega), \quad j = 0, 1, 2, \ldots,$$

and this can be written as a sum of delta functions

$$E(\omega, m) = S_0 \delta[m - m_0(\omega)] + S_1 \delta[m - m_1(\omega)] + \ldots$$

The continuum is concentrated in a narrow wedge adjoining the "ray" of normal incidence, $m_n = m_n(\omega)$, so that, with good approximation, we can use the expression $S_n \delta[m - m_n(\omega)]$ for the continuum. We can then replace the integrals in equations (9) by the summations

$$S = S_n + \sum_{j=0}^{\infty} S_j + N,$$

$$S' = S_n \cos^2 m_n x' + \sum_{j=0}^{\infty} S_j \cos^2 m_j x' + N', \qquad (10)$$

$$C = S_n \cos m_n x' + \sum_{j=0}^{\infty} S_j \cos m_j x',$$

$$Q = 0,$$

where S is the onshore spectrum ($x = 0, y = 0$) and S' the offshore spectrum ($x = x', y = 0$). The dependence of S, S', C, Q and m on frequency is understood.

EFFECT ON COHERENCE. First we consider the loss of coherence due to multiple in-phase modes, neglecting noise. Take the case near $\omega = \frac{1}{2}\pi$. Then

$$S = S_n + S_0, \quad S' = S_n \cos^2 m_n x' + S_0 \cos^2 m_0 x',$$
$$C = S_n \cos m_n x' + S_0 \cos m_0 x', \quad Q = 0,$$

and

$$R^2 = \frac{C^2}{S S'} = 1 - \frac{S_n S_0 (\cos m_n x' - \cos m_0 x')^2}{(S_n + S_0)(S_n \cos^2 m_n x' + S_0 \cos m_0 x')}.$$

Thus $R^2 = 1$ for either $S_n = 0$ or $S_0 = 0$. Setting $S_n = S_0$ and using the numerical values $m_n = 90°$, $m_0 = 72°$, $x' = 0.4$ yields $R^2 = 0.995$. The loss of coherence is negligible.

Next set $S_0 = 0$, $N = N'$, and $\cos m_n x' = 1$. This gives

$$R^2 = \frac{S_n}{S_n + N}.$$

The observed value, $R^2 = 0.87$, then indicates that about 13% of the wave record is due to incoherent noise at the two stations. This may be due in part to atmospheric pressure oscillations (see *Conclusions*).

Finally we consider the coherence near the phase reversal. If there is normal incidence only, $S = S_n$, then the coherence beyond the reversal recovers to $R^2 = 1$ in the absence of noise (Fig. 12); similar remarks apply to $S = S_0$ only. In the presence of noise we should expect the coherence to approach the level prior to reversal. In fact it remains at a much lower level. This is the expected result if two or more modes are present.

For illustration, set $S = S_n + S_o$ with $S_n = 2S_o$. Then

$$S = 3S_o, \quad S' = (2\cos^2 m_n x' + \cos^2 m_o x')\, S_o$$

and

$$R^2 = \frac{(2\cos m_n x' + \cos m_o x')^2}{3\,(2\cos^2 m_n x' + \cos^2 m_o x')}.$$

The resulting curve in Fig. 13 illustrates how the continuum and the fundamental mode conspire to prevent recovery of coherency for frequencies above those of the phase reversal. Numerical values are about as observed.
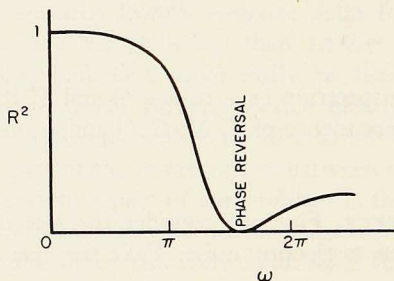

Figure 13. Coherence versus frequency for the case $S_n = 2S_o$.

At frequencies just above $\omega = 2\pi\,(\sim 1.2\ \text{cph})$, the coherency rises to about the same high value as below the first reversal frequency. Reference to Fig. 10 suggests the possibility that the combined out-of-phase energy of the continuum and the modes $j = 1, j = 2$ now sufficiently exceed the in-phase energy of $j = 0$ to bring this situation about. With sufficient effort (and optimism) even the numerical values can be reproduced.

PHASE REVERSALS. Consider the situation at $\omega = \pi$. At this frequency there exists only one discrete mode, $j = 0$, and its normal-to-shore wave number, m, is slightly less than $\frac{1}{2}\pi$. The continuum is contained between $m = 0.9\,\pi$ and $m = \pi$. Hence all energy is associated with wave numbers below $1.25\,\pi$, for which $\cos mx'$ is positive. Hence C is positive, and the two instruments are in phase, as observed.

Next consider a frequency, ω_r, slightly above $1.25\,\pi$ [just above (2) in the figure]. The continuum associated with near-normal incidence is out of phase, whereas the continuum associated with near-glancing incidence is in phase. There are now two possible discrete modes, $j = 0$ and $j = 1$, and both of these are in phase. The observed phase reversal, if properly interpreted, states that the total *weighted* out-of-phase energy exceeds the total in-phase energy

$$\int_{1.25}^{\infty} \cos mx' \, S(\omega_r, m) \, dm > \int_{0}^{1.25} \cos mx' \, S(\omega_r, m) \, dm \, .$$

One is tempted to interpret the phase notch between 0.8 and 0.9 cph in terms of the vicinity to ω_r, the cut-off frequency for $j = 1$. The argument is as follows: It is conceivable that with increasing frequency the balance be reversed in the sense that the energy of the two discrete modes exceed the energy of the continuum. In that event φ would go back to 0° at some frequency such as that marked (5). At $\omega = 1.39\,\pi$ [point (6)] the discrete mode $j = 1$ has a node at the offshore instrument. For slightly larger frequencies the continuum plus the $j = 0$ mode are now reversed, and only $j = 1$ is in phase. This could lead to a restoration of the out-of-phase relation. Let S_n, S_0, S_1 be the energies associated with near-normal incidence and the discrete modes $j = 0$ and $j = 1$ respectively. Furthermore assume that the cut-off frequency for $j = 1$ is slightly above $1.25\,\pi$ (the theoretical cut-off for the step topography is at frequency π). Then we have (Fig. 10)

$$\begin{array}{lll} \text{out-of-phase} & \text{between (2) and (5):} & S_0 < S_n \, , \\ \text{in-phase} & \text{between (5) and (6):} & S_0 + S > S_n \, , \\ \text{out-of-phase} & \text{beyond (6)} & S_0 < S_n + S_1 \, . \end{array}$$

The inequalities cannot be satisfied unless the discrete and continuous spectra contain comparable energy.

Quantitatively the above suggestion leaves much to be desired. The observed notch between (5) and (6) is wider and at higher frequencies than would be consistent with the theory for the step topography. Still it is difficult to see how the complex phase relation could exist unless both the discrete and continuous spectrum contributed appreciably to the total spectrum.

PARTIAL ABSORPTION. Suppose a fraction $1 - s^2$ of the energy is absorbed as the wave travels from the offshore to the onshore recorder. Let $\frac{1}{2}a$ be the incident amplitude offshore; then $\frac{1}{2}sa$ is the amplitude of the incident and reflected waves as measured near the shoreline, $s(\frac{1}{2}sa)$ the reflected amplitude offshore. Thus a fraction $1 - s^4$ is dissipated on the round trip. For an elementary wave train we have

$$\eta(0, t) = sa \cos \omega t \, ,$$
$$\eta(x, t) = \tfrac{1}{2} a \cos (mx + \omega t) + \tfrac{1}{2} s^2 a \cos (mx - \omega t) \, .$$

Proceeding as previously we find

$$\begin{array}{ll} S & = \tfrac{1}{2} s^2 a^2 \, , \\ S' & = \tfrac{1}{2} s^2 a^2 \cos^2 mx + \tfrac{1}{8}(1 - s^2)^2 a^2 \, , \\ C & = \tfrac{1}{4} s(1 + s^2) a^2 \cos mx \, , \\ Q & = \tfrac{1}{4} s(1 - s^2) a^2 \sin mx \, , \end{array}$$

and this yields

$$\tan \varphi = \frac{1 - s^2}{1 + s^2} \tan mx , \quad R^2 = 1 . \tag{11}$$

Fig. 14 shows the relation for selected values of s. The ordinate is proportional to frequency, and for normal incidence $mx = 0.4 \, \omega$. Perfect reflection ($s^2 = 1$) yields the abrupt phase reversal previously discussed. Perfect absorption leads to a linear increase of phase with frequency. The observed behavior is more
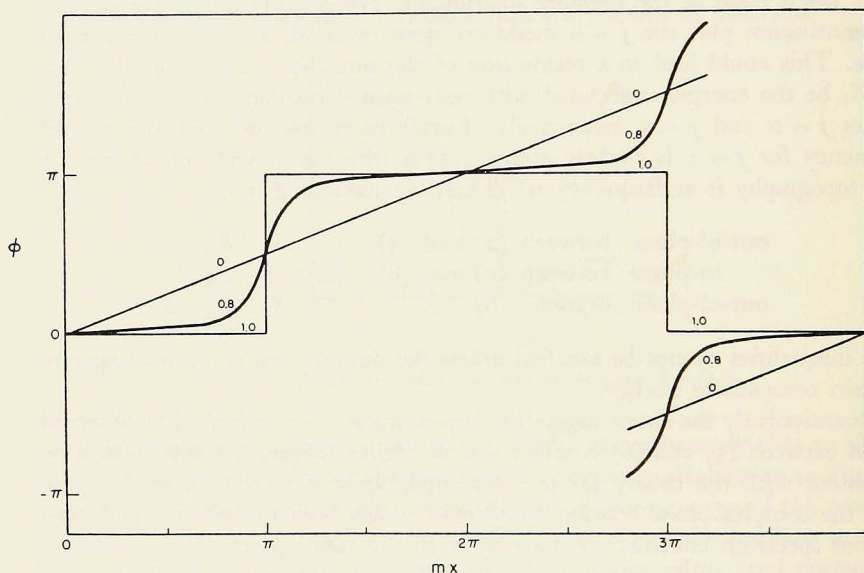

Figure 14. Phase versus mx ($\sim \omega$) for various values of absorption. Here $s^2 = 1$ refers to no absorption of energy between stations; $s^2 = 0$ to complete absorption.

nearly in accord with perfect reflection. The curve $s^2 = 0.8$ (energy dissipation, $1 - s^4 = 0.36$) is somewhat comparable with the observed lack of abruptness in the phase transition, but it must be regarded as an upper limit inasmuch as some of the transition softening is related to lack of frequency resolution. The technique could be developed to yield meaningful estimates of coastal reflectivity.

DISTRIBUTED REFLECTORS. Suppose the coast reflects perfectly, but on account of coastal irregularities the distance from the offshore instrument is variable. The effect is somewhat the same as if we replaced the distance, x, of the offshore instrument by a probability distribution $P(\xi) \delta \xi$ of the distance lying between $x + \xi - \frac{1}{2} \delta \xi$ and $x + \xi + \frac{1}{2} \delta \xi$. Let $\xi \langle\langle x$. Then we have

$$S = \tfrac{1}{2} a^2 ,$$
$$S' = \tfrac{1}{2} a^2 \left(\cos^2 mx - m^2 \, \overline{\xi^2} \cos 2mx \right) ,$$
$$C = \left(1 - m^2 \, \overline{\xi^2} \right) \cos mx ,$$
$$Q = 0 ,$$

where $\overline{\xi^2}$ is the variance of ξ. The coherency equals

$$R^2 = 1 - m^2 \, \overline{\xi^2} \tan^2 mx + \ldots ,$$

and this would lead to an appreciable loss of coherence. The phase relation is unaffected.

LONGSHORE SEPARATION. The two stations are not located along a line normal to shore (as assumed in the discussion), San Clemente being about 50 km north of La Jolla (Fig. 1). What is the effect of this displacement on phase and coherence?

Going back to equation (9) we write

$$\Delta y = y_2 - y_1 = \frac{50 \text{ km}}{250 \text{ km}} = 0.2$$

for the dimensionless separation (as a ratio of shelf width). Suppose energy were concentrated in any one mode. Then on forming the ratio Q/C we obtain $\tan \varphi = \tan n\Delta y$, or $\varphi = n\Delta y$. Consider the case for the second reversal, at $\omega = 9.2$. Observations indicate that San Clemente lags La Jolla by $220°$, as compared to $180°$ for perfect reflection. If this additional phase lag of $40° = 0.7$ radians were due to the longshore separation, then $n = \varphi/\Delta y = 0.7/0.2 = 3.5$. The values $\omega = 9.2$, $n = 3.5$ are consistent with incidence from the south very near glancing incidence, $\theta' = 80°$.

The coherency is not affected under the present assumption. But if we permit a wave to travel in either direction, then the situation is different. Let E designate the energy of waves from south to north and $s^2 E$ the energy from north to south, again under the assumption of a single mode. Then

$$S_{11} = (1 + s^2) E , \qquad\qquad S_{22} = (1 + s^2) E \cos^2 mx ,$$
$$C_{12} = (1 + s^2) E \cos mx \cos n\Delta y , \qquad Q_{12} = (1 - s^2) E \cos mx \cos n\Delta y ,$$

$$\tan \varphi = \frac{1 - s^2}{1 + s^2} \tan n\Delta y \tag{12}$$

$$R^2 = 1 - \frac{4 s^2}{(1 + s^2)^2} \sin^2 n\Delta y . \tag{13}$$

The phase relation is analogous to that due to partial absorption (11) as portrayed in Fig. 14. The transition is centered at $n\Delta y = \pi$; the suddenness is determined by the value of s. The inferred value of longshore wave number

at the transition is $n = \pi/\Delta y = 5$. The observed frequency of transition is $\omega = 3.7$. These values are inconsistent with any possible solution (see Fig. 8), and it is concluded that the phase reversals are not due to interference from oppositely traveling waves in the y-direction.

In a previous investigation (Munk, *et al.*, 1959: chart 10.2) it was found that the coherence between La Jolla and Oceanside, California ($\Delta y = 0.13$) diminished with increasing frequency roughly as $R^2 = 1 - \sin^2 (0.11\ \omega)$ until it vanished, but did not rise with increasing frequencies. Comparison with (13) suggests $s^2 \approx 1$, *i. e.*, almost equal energy traveling in both directions. From (13) we then find that the coherence should vanish for $n = \frac{1}{2}\ \pi/\Delta y \approx 4\pi$. Consider a vertical line drawn on Fig. 9 for $n = 4\ \pi$. For frequencies of about $1.5\ \pi$ or less, all possible solutions are in phase, and the expected coherence is high. The observed loss of coherence occurs at $\omega = \frac{1}{2}\ \pi/0.11 \approx 4.5\ \pi$; at this frequency the continuum for incidence more nearly normal than Brewster's angle is in phase, whereas the waves near glancing incidence and the discrete modes ($j = 0, 1, 2, 3$) are all out of phase. Again the loss of coherence can be interpreted as an indication of comparable energy in the continuum (concentrated near normal incidence) and in the discrete modes.

12. *Conclusions.* The most prominent observed features are the phase reversals at 0.6 and 1.7 cph, and these are not inconsistent with simple standing wave patterns over the continental borderland. Resonant amplification (in the open-organ pipe sense) leads to the spectral peaks at the coast line. The situation is then quite analogous to the resonance amplification of the lunar semidiurnal tide over the broad Atlantic shelf (Redfield, 1958).

Unfortunately the picture is not this simple. There is strong evidence that radiation from the open sea cannot be the only source of the recorded oscillations on the borderland. If it were, then all wave motion at the two recorders should be in phase at frequencies below that of reversal and out of phase at frequencies above phase reversal, except for a narrow transition band centered on the frequency of phase reversal. The coherency is a measure of the relative phase, and it would then show a narrow trough centered at phase reversal and be equally high on both sides. In fact the coherency is much lower at the high-frequency side of the phase reversal. The interpretation is as follows: on the low-frequency side, all energy associated with any fixed frequency is in phase at the two instruments; on the high-frequency side, most of the energy is out of phase, but a substantial fraction remains in phase.

There is a straightforward way out of this dilemma. The "continuous spectrum" associated with radiation from the open sea is only one of the two classes of solutions to the pertinent boundary value problem. In addition to this continuum there are solutions corresponding to the discrete modes, or edge waves. The existence of these would produce just the effect here indicated. Thus the lowest mode, $j = 0$, remains in phase at all frequencies and

could be responsible for the low coherence above the reversal frequency if it contained about half the energy of the continuous spectrum.

The trouble is that, once the superposition of continuous and discrete modes of equivalent energy is admitted, the situation is sufficiently complex that nearly any observations can be accounted for. Thus a bothersome "notch" in the phase diagram can be attributed to the mode $j = 1$ which is initially formed in phase and which, with increasing frequency, passes out of phase. We also wish to refer to the complex and remarkably reproducible cross-spectra previously obtained off Guadalupe Island (Fig. 4) and to two similar analyses of lesser quality off the California coast (Munk, *et al.*, 1959). In those instances the separation between the offshore and onshore instruments was 1.5 km (as compared to 100 km in the present case), and the phase reversals took place at much higher frequencies. It turns out that the observed spectral features are inconsistent with edge-wave theory only, or continuum theory only. We intend to study these cases further. The comparison of records obtained from instruments separated at various distances longshore is planned for later this year.

At this time we conclude that the continuum and discrete spectra are of the same order. If the coast were truly one-dimensional, $h = h(x)$, then the continuum would naturally be ascribed to pressure and wind fluctuations over the open sea, and the edge waves to similar meteorological disturbances over or near the borderland. But the coastline is complex, and we must expect the scattering of energy from any one mode to any other. One may envision that the scattering processes would bring about compatible distributions of energy among all modes, regardless of whether disturbances in the open sea or over the borderland are the ultimate cause.

From the observations over the borderland we may infer the spectrum in the deep sea. It appears to be flat at frequencies above 0.7 cph, with an energy density of roughly 10^{-2} cm²/cph, and this is not inconsistent with previous measurements off Guadalupe Island. At frequencies below 0.7 cph the spec-
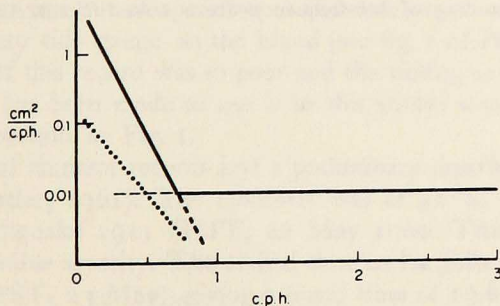

Figure 15. The deep-sea spectrum (devoid of shelf resonances). The dotted line is the spectra level indicated from atmospheric pressure measurements.

trum rises sharply. It is reasonable to suppose that the inferred deep-sea spectrum is due to a superposition of two processes: one leading to the $f-3$ spectrum which dominates at the low frequencies; the other to the flat spectrum which dominates at the high frequencies. This is sketched on Fig. 15. The dotted line is the spectrum of atmospheric pressure in $(mb)^2/cph$, according to Gossard (1960). A millibar (mb) and a centimeter (cm) of water are equivalent pressure units, and the curves are on a comparable scale. If the sea level is considered fixed, then the pressure transducer on the sea bottom would presumably record oscillations associated with the atmospheric pressure spectrum. If the sea level yields in the sense of an inverted barometer, then the pressure fluctuations on the sea bottom would vanish. The observed fact is that the recorded fluctuations are larger by an order of magnitude than those due to atmospheric pressure, and this eliminates atmospheric pressure *in situ* as the principal cause of the recorded oscillations. Some of the loss of coherence at low frequencies may, however, be due to *in situ* atmospheric pressure effects.

We wish to acknowledge the suggestions received from Carl Eckart, Norman Barber, and George Backus.

REFERENCES

GOSSARD, E. E.
    1960. Spectra of atmospheric scalars. J. geophys. Res., 65 (10): 3339–3351.
MARTIN, M. A.
    1957. Frequency domain applications in data processing. General Electric, Techn. Inf. Ser. 57 SD 340.
MUNK, W. H., F. E. SNODGRASS, and M. J. TUCKER
    1959. Spectra of low-frequency ocean waves. Bull. Scripps Inst. Oceanogr., 7: 283–362.
REDFIELD, A. C.
    1958. The influence of the continental shelf on the tides of the Atlantic coast of the United States. J. Mar. Res., 17: 432–448.
SNODGRASS, F. E.
    1961. Digital recording of waves and tides (In preparation).
SNODGRASS, F. E., W. H. MUNK, and M. J. TUCKER
    1958. Offshore recording of low-frequency ocean waves. Trans. Amer. geophys. Un., 39: 114–120.